# On the Structure of the Thiolated Au130 Cluster.

**ARTICLE** *in* THE JOURNAL OF PHYSICAL CHEMISTRY A · SEPTEMBER 2013

Impact Factor: 2.69 · DOI: 10.1021/jp406665m · Source: PubMed

THE JOURNAL OF PHYSICAL CHEMISTRY A

Article

pubs.acs.org/JPCA

# Structure of the Thiolated $Au_{130}$ Cluster

Alfredo Tlahuice-Flores,[†] Ulises Santiago,[†] Daniel Bahena,[†] Ekaterina Vinogradova,[†] Cecil V. Conroy,[§] Tarushee Ahuja,[§] Stephan B. H. Bach,[‡] Arturo Ponce, Gangli Wang,[§] Miguel José-Yacamán,[†] and Robert L. Whetten*,[†]

[†]Department of Physics and Astronomy and [‡]Department of Chemistry, University of Texas at San Antonio, One UTSA Circle, San Antonio, Texas 78249, United States

[§]Department of Chemistry, Georgia State University, P.O. Box 3965, Atlanta, Georgia 30302-3965, United States

Supporting Information

**ABSTRACT:** The structure of the recently discovered $Au_{130}$-thiolate and -dithiolate clusters is explored in a combined experiment-theory approach. Rapid electron diffraction in scanning/transmission electron microscopy (STEM) enables atomic-resolution imaging of the gold core and the comparison with density functional theory (DFT)-optimized realistic structure models. The results are consistent with a 105-atom truncated-decahedral core protected by 25 short staple motifs, incorporating disulfide bridges linking the dithiolate ligands. The optimized structure also accounts, via time-dependent DFT (TD-DFT) simulation, for the distinctive optical absorption spectrum, and rationalizes the special stability underlying the selective formation of the $Au_{130}$ cluster in high yield. The structure is distinct from, yet shares some features with, each of the known $Au_{102}$ and $Au_{144}/Au_{146}$ systems.

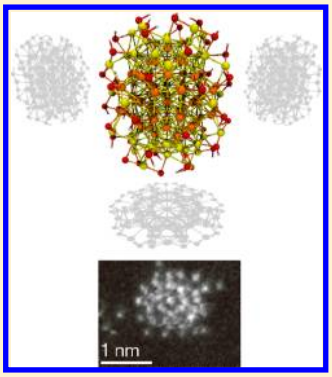


## 1. INTRODUCTION

Gold nanoparticles protected by thiolate ligands have attracted extensive research activity because of their enhanced optical, electrochemical, and other application-related properties. The desired physicochemical properties are strongly dependent upon size, composition, and structure. It is therefore critical for improved materials design to correlate the cluster structure and bonding with the properties sought for applications.

However, the determination of atomic structures of nanomaterials is a challenging task even for composition elucidated gold−thiolate nanoclusters where gold cores span various symmetries.[1−4] In the case of thiolate protected gold clusters comprising more than 100 gold atoms, the solved structure of the $Au_{102}(SR)_{44}$ cluster represented a breakthrough in our knowledge of the structure principles. Single-crystal X-ray diffraction revealed that the core morphology of $Au_{102}(SR)_{44}$ is an $Au_{79}$ Marks decahedron with two 15-gold rings located at its poles and covered by 19 short -SR-Au-SR (monomer), and 2 long -SR-Au-SR-Au-SR- (dimer) motifs.[5] The solved core structure held a $D_5$ point group (0.4 Å tolerance) with a $C_5$ axis along its main axis.[6,8] Another amply studied structure is the $Au_{144}(SR)_{60}$ cluster which represents a high *I*-symmetry structure.[9−11] Recently we have shown that its 5-fold axes were found most of the time during a scanning/transmission electron microscopy (STEM) study.[12] Noteworthy is that as the size of thiolate-protected gold clusters increase then the main core resembles the gold in bulk or a Marks decahedron.[13,14]

Recently, Wang and co-workers reported the synthesis of a novel thiolate protected gold cluster with outstanding stability, optical and electrical properties in which compositionally both dithiolates (∼30 durene-dithiols) and monothiolates (∼ 20 phenyl-ethane thiols) are present in the protective monolayer. The compositional and mass spectrometric evidence supported a formulation as ∼ $Au_{130}(SR)_{50/80}$,[15] where the subscript indicates the count of thiolate sulfur originating in either mono- or dithiolate. The Au-thiolate bonding interactions were investigated by the early stage reactions at the core-ligand interfaces between the thiolate ligands and excess thiols, through which the dithiols were found to replace monothiolate ligands at 1:2 stoichiometry ratio, while addition of monothiols into dithiolate monolayer instead of exchange was observed.[16,17] No direct evidence of the core structure has been reported, but plausible models are indicated by the similar formula of the $Au_{130}(SR)_{50}$ monothiolate compound recently reported by Negishi et al.,[18] and by the proximity to the established monothiolate compounds $Au_{102}(SR)_{44}$ and "ubiquitous" $Au_{144/146}(SR)_{60}$.

In this paper we report a combined experimental and theoretical investigation of the structure of the $Au_{130}(SR)_{50/80}$ cluster, hereafter denoted simply as "$Au_{130}$". We use a theoretical approach based on density functional theory (DFT) to perform the structural relaxation of the $Au_{130}(SH)_{50}$ cluster and mixed dithiolate clusters, starting from a concept proposed by Negishi et al.[18] to explain the cluster of definite composition $Au_{130}(SC_{12}H_{25})_{50}$. Experimen-

**Received:** July 5, 2013
**Revised:** August 10, 2013
**Published:** September 4, 2013

   dx.doi.org/10.1021/jp406665m | *J. Phys. Chem. A* 2013, 117, 10470−10476

tally, the structural characteristics were determined by using aberration corrected Scanning Transmission Electron Microscopy (STEM) and Electron diffraction on the STEM mode. The proposed structure is supported by the good agreement between the measurement of the sample and calculated absorption spectrum. In addition, we found good matching between experimental diffraction patterns and the simulated ones of a model relaxed by DFT calculations.

## 2. EXPERIMENTAL METHODS AND MATERIALS

**Materials.** Durene-$\alpha$1-$\alpha$2-dithiol (durene-dithiol) was from TCI America. Other chemicals were from Sigma. All materials were used as received.

**Synthesis.** The $Au_{130}$ nanoclusters were synthesized following previously published literature.[15] Briefly, gold salt ($HAuCl_4 \cdot 3H_2O$, >99.9%) dissolved in water was phase transferred into toluene phase using tetraoctylammonium bromide (TOABr, 98%) as transfer agent. After discarding the aqueous layer, a toluene solution containing mixed thiols, durene-$\alpha$1-$\alpha$2-dithiol (durene-dithiol, >95%), and phenylethyl mercaptan (phenyl-ethane thiol, ≥99%) was added to the organic layer. The overall mole ratio of Au:durene-dithiol:-phenyl-ethane thiol was 1:1:2. After being stirred for 30 minutes until the solution turned colorless, the solution was cooled in an ice bath and reduced by quick addition of chilled sodium borohydride ($NaBH_4$, >99%) (20 equivalents relative to gold) aqueous solution under rapid stirring. After 3 days, the reaction mixture was washed with water thrice and solvent evaporated to dryness. The solid was washed with copious methanol followed by acetonitrile to remove remaining free ligands (confirmed by $^1$H NMR). Final product can be reconstituted in dichloromethane repeatedly.

The $Au_{130}$ nanocluster sample was characterized using UV−visible spectroscopy. The spectra were recorded on a Varian-Cary 5000 spectrophotometer in the double beam mode. Scans were run from 200 to 800 nm at a scan rate of 600 nm/min, a data interval of 1 nm, and the slit at full height. The experimental absorption spectrum is provided in the Supporting Information, Figure S1. All the mass spectra were acquired on an Ultraflextreme (Bruker Daltonics, Billerica, MA) matrix assisted laser desorption ionization (MALDI) time-of-flight (TOF) mass spectrometer using the linear positive-ion mode. The following instrument source parameters were used: ion source 1 25 kV, ion source 2 23.05 kV, lens 6.5 kV and pulsed ion extraction (PIE) 300 ns. The matrix suppression cutoff mass was set to 8000 Da. The laser beam focus was set at 35, and 6000 shots were averaged for each spectrum (Supporting Information, Figure S3). Mass calibration was done using the Protein 2 Calibration Standard (Bruker Daltonics part no. 207234). The matrix used was *trans*-2-[3-(4-*tert*-butylphenyl)-2-methly-2-propenylidene malononitrile (DCTB, [300364-84-5], catalog no. 727881, = 98%). MALDI samples were prepared using the mixed drop method on a stainless steel MALDI plate. The matrix was prepared in chloroform at a concentration of 20 mM. Ten microliters of the $Au_{130}$ cluster solution (in either dichloromethane (DCM) or toluene) was added to 10 $\mu$L of the DCTB matrix solution in a small spin tube and mixed thoroughly to generate a 2000:1 ratio between matrix and analyte. The spot was allowed to dry in a vacuum desiccator before loading into the MALDI TOF.

Raman spectra were measured with an iHR 320 Horiba Jobin Yvon spectrometer equipped with a thermoelectrically cooled charge coupled detector (Synapse CCD Detection System) operating at −70 °C and an Olympus BX41optical microscope. This instrument facilitates laser excitation with a wavelength at 785 nm through a 10× microscope objective. This results in a laser spot diameter of approximately 3.8 $\mu$m. The signal was calibrated by using the 520 $cm^{-1}$ line of a silicon wafer. For the Raman measurements, 10 $\mu$L of an analyte solution was deposited onto a quartz slide and dried at room temperature. Five to eight SERS spectra were measured using 25 mW of laser power and a 500 $\mu$m slit aperture for a 10 s exposure time at different illumination spots for each sample. Spectra were collected and processed using the Horiba Scientific's LabSpec 6 software.

In the present work, we have used STEM-Diffraction to experimentally observe diffraction patterns of a single cluster. This technique is challenging at the nanoscale for different cluster nanostructures. With this methodology we determined the structure of the $Au_{130}$ cluster following a similar procedure as reported for the $Au_{144}(SR)_{60}$ cluster.[12] This procedure is more accurate for resolving small structures less than 3 nm when compared with powder X-ray patterns. The TEM/STEM sample grid was prepared by placing 3 drops of dilute solution on a holey carbon film coated Cu grid (3 mm, 300 mesh) and dried under room temperature in a glass Petri dish to evaporate it slowly, and promote better dispersion onto the carbon film. The HAADF STEM images and nanobeam diffraction (NBD) patterns were recorded using a probe Cs-corrected JEOL JEM-ARM 200F operated at 80 kV. The images were obtained with a convergence angle of 26 mrad and the collection semiangles from 50 to 180 mrad. The probe size used was about 0.09 nm with a probe current of 22 pA.

## 3. THEORETICAL METHODS

We use a theoretical approach based on DFT to perform the structural relaxation of the $Au_{130}(SH)_{50}$ cluster based on a concept proposed by Negishi et al.[18] to explain the cluster of definite composition $Au_{130}(SC_{12}H_{25})_{50}$. The initial structure was considered relaxed when a 0.01 eV/Å value in force was obtained. During the optimization stage, hydrogen atoms bound to the sulfur atoms orient themselves into cis and trans positions yielding a final $C_5$-symmetry that was verified by applying a 0.1 Å tolerance in position of the Cartesian coordinates. The methodology of the optimization stage uses a double-$\zeta$ polarized basis set, the Perdew−Burke−Ernzehorf (PBE) parametrization for the exchange-correlation functional,[19] within the generalized gradient approximation (GGA), and the Troullier−Martins scalar relativistic norm-conserving pseudopotentials,[20] as implemented in the SIESTA package.[21]

For the calculation of the optical spectrum, we used a real-time method within TD-DFT,[22] as implemented in the octopus code.[23,24] To calculate singlet excitations in the low energy region (1.0−4.0 eV), we use the TD-LDA approximation and the Perdew−Zunger exchange-correlation functional.[25] Briefly, we yield the optimized structure in SIESTA to the octopus code where a ground state calculation is performed to get the electron density. The system is then perturbed by a short electrical pulse. When the perturbation is turned off, the time-dependent evolution of the dipole moment of the system is followed. During the calculation of the absorption spectra the electric dipole moment of the system and the imaginary part of its dynamical polarizability are evaluated. The real space method is used, and we consider a spacing of 0.2 Å. The simulation box is formed by adding spheres of 3.5 Å around


dx.doi.org/10.1021/jp406665m | J. Phys. Chem. A 2013, 117, 10470−10476

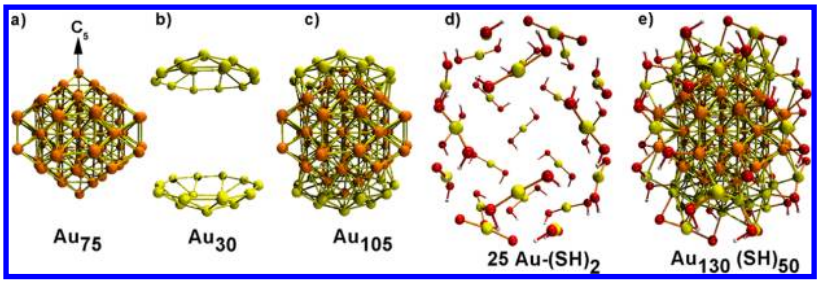


**Figure 1.** Optimized model for $Au_{130}(SH)_{50}$ cluster oriented along a vertical $C_5$-axis, obtained through the use of first-principles DFT optimization. (a) The inner core is an $Au_{75}$ Marks decahedron (orange); (b) two 15-atom rings (yellow) cap the $Au_{75}$ core; (c) The complete $Au_{105}$ grand core; (d) The 25 gold adatoms (also yellow) form part of the monomer (HS-Au-SH) motifs; (e) The full structure of the $Au_{130}(SH)_{50}$ cluster, where S and H atoms forming the ligands are shown as red and white spheres, respectively.

each atom. The time dependent equations were integrated considering a maximum time step of 0.002 $\hbar$/eV, that is, 0.00132 fs.

## 4. RESULTS AND DISCUSSION

**4.1. Model of the Thiolate-Protected $Au_{130}$ Cluster.** Currently, theoretical calculations of thiolate-protected gold clusters utilize DFT to get good matching with structural properties. Following this line, in this report we have used DFT and time dependent DFT (TD-DFT) methodologies to propose one structure in agreement with the experimental results (HAADF-STEM images). It is important to mention that the proposed model follows the experimental evidence: (a) Cluster composed of more than 100 gold atoms are covered preferentially by short motifs given the high curvature of their surfaces, (b) HAADF-STEM images have shown the 5-fold symmetry as more preponderant during our experiments, and (c) The stability of big sizes need not necessarily comply with a closed electron-shell, but their stability might be attributed to geometric effects.

The $Au_{130}$ clusters contain 130 gold atoms and a varying number of sulfur atoms (50 or 80) depending on the type of ligands (pure monothiols or a mixture of mono- and dithiols).[15,16,18] However, given the evidence that in the ligand exchange reaction in the $Au_{25}(SR)_{18}$ cluster, the dithiol molecules are incorporated in such a way that the thiolated $Au_{25}$ cluster preserves its electronic and optical features. This implies that the dithiolate ligands are not perturbing the gold core significantly.[26] However, in the case of durene-dithiolates, which have accessible energy states and steric confinement, the effect of dithiolate may be significant.[17] In this study, we have computationally relaxed two models independently, one for $Au_{130}(SH)_{50}$ and one for $Au_{130}[(SH)_2]_{10}[(SCH_2CH{=}CHCH_2S)_2]_{15}$, to simulate the HAADF-STEM images of the cluster with 50/80 sulfur atoms, thus finding good agreement with experimental data.

The $Au_{130}(SH)_{50}$ cluster consists of an $Au_{105}$ core which can be seen as an $Au_{75}$ Marks decahedron (Figure 1a) which is capped with two $Au_{15}$ rings (Figure 1b) along its $C_5$ axis. Additional gold atoms (adatoms) are included in the 25 monomer motifs (HS-Au-SH) which are protecting the $Au_{105}$ grand core (Figure 1d–e). The monomer motifs are distributed as follows: 10 monomer motifs are located at the ending (or poles) of the elongated $Au_{105}$ grand core and 15 are located at the equatorial positions forming patterns around the square faces of the inner $Au_{75}$ core. There are 55 Au atoms not in direct bonding to sulfur, having the morphology of a truncated (Ino-type) decahedron. The relaxed structure shown in Figure 1 contains a $C_5$ point group (0.1 Å tolerance in position), which increases to $D_5$ by considering a 0.6 Å tolerance. More complicated ligands (those including steric effects) might perturb the gold adatoms located at its equatorial region and therefore impact the five perpendicular $C_2$ axes which passes through them. In those structures we expect that a reduced $C_5$ point group might at least be maintained. Further rotation of the monomer motif patterns around the square faces of $Au_{75}$ might produce its corresponding enantiomer.

The calculated bond lengths (Figure 2) of the $Au_{130}(SH)_{50}$ cluster are composed of 50 S–H bonds (1.38–1.39 Å), 50

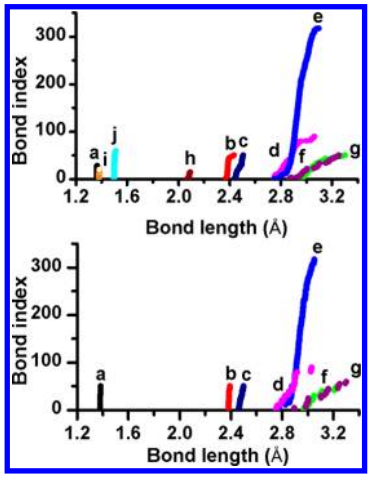


**Figure 2.** Calculated interatomic distances. The different distances are labeled as follow: **a** S–H bonds (black); **b** Au(adatom)-S distances (red); **c** Au(core)-S distances (dark blue); **d** bond distances between $Au_{75}$ and $Au_{15}$ rings (pink); **e** $Au_{75}$ Marks decahedron bond distances (blue); **f** Au(core)-Au(adatom) (green); **g** $Au_{15}$ rings (purple). Upper graph shows the $Au_{130}$ cluster with 80 S atoms, label **h** is for S–S bonds; **i** is for C=C bonds and **j** represents C–C bonds.

Au(adatom)-S bonds (2.38–2.39 Å), and 50 Au(core)-S(monomer) bonds linking the 25 monomer motifs to the $Au_{105}$ core (2.46–2.50 Å). The Au–Au bonds are distributed as follows: 317 Au–Au bonds forming the $Au_{75}$ core between 2.78–3.05 Å; 50 Au–Au bonds which are part of the two $Au_{15}$ rings between 2.97–3.23 Å; 90 Au–Au bonds linking the $Au_{75}$ inner core with the $Au_{15}$ rings (2.75–3.0 Å); 60 Au(core)-Au(adatom) bonds which bind the 25 monomer motifs to the $Au_{105}$ core between 2.9–3.3 Å. Note that the $Au_{130}[(SH)_2]_{10}[(SCH_2CH{=}CHCH_2S)_2]_{15}$ structure (Supporting Information, Figure S4) is an extension of the $Au_{130}(SH)_{50}$ cluster, where each of the equatorial monomer motifs link two dithiolate groups in an intrastaple mode (15 times 4 S atoms)


dx.doi.org/10.1021/jp406665m | J. Phys. Chem. A 2013, 117, 10470–10476

and each of the monomer motifs located at the ends hold 2 (aliphatic) ligands (10 times 2 S atoms). Thus, the proposed $Au_{130}[(SH)_2]_{10}[(SCH_2CH{=}CHCH_2S)_2]_{15}$ model involves disulfide bonds between the dithiolate ligands. This assumption was supported by a comparison of the Raman spectra obtained from samples of the $Au_{144}(SR)_{60}$ and the $Au_{130}$ clusters. The $Au_{130}$ samples show a small but significant Raman active peak which is located at the expected position (ca. 500 $cm^{-1}$) of the disulfide bond, while it is not found in the $Au_{144}(SR)_{60}$ samples (Supporting Information, Figure S5).

Regarding the absorption spectrum of the $Au_{130}$ cluster. A comparison between the experimental and calculated absorption spectra is shown in the Figure 3. Both spectra show

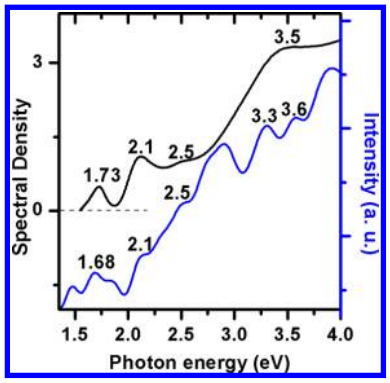


**Figure 3.** Comparison between the experimental (black curve) and the calculated (blue curve) $Au_{130}(SH)_{50}$ absorption spectrum by TD-DFT.

coincident peaks located at 1.7, 2.1, and 2.5 eV. In the region between 2.5−4.0 eV a peak located at 3.5 eV is observed, while a peak located at 3.6 eV is present in the calculated spectrum. In addition, we have calculated the optical absorption spectrum for the $Au_{130}[(SH)_2]_{10}[(SCH_2CH{=}CHCH_2S)_2]_{15}$ cluster, and it is provided in the Supporting Information, Figure S2. This spectrum shows similar features located at 1.72, 2.1, and 2.4 eV with slight differences located between 2.5−4.0 eV. We attribute those differences to ligand effects, as it has been indicated previously for the thiolated $Au_{25}$ cluster.[27]

**4.2. STEM-Diffraction.** The structure of the $Au_{130}$ cluster was solved by the comparison of the experimental STEM diffraction patterns with the simulated ones of the $Au_{130}$ model described above. In the nanobeam diffraction (NBD), through the STEM imaging mode we are able to reduce the radiation damage to the clusters by using an energy reduction from 80 kV.

A series of diffraction patterns were obtained by focusing the beam each time on a specific particle (with relative orientation) and merged as a video (available as video 1 in the Supporting Information). Figure 4 illustrates an individual frame of the NBD experiment. First, we collect the HAADF image (Figure 4a) and then stop the scanning to collect the diffraction pattern. We then move the beam to each single cluster as shown by the arrow. Figure 4b shows the diffraction pattern of a single cluster. It is noteworthy that our reported method preserves the symmetry of the studied clusters, and obtained patterns are employed for a straight comparison with the simulated ones using a DFT relaxed model. A full atlas of the simulated diffraction patterns and a map of images of the model proposed are presented in the Supporting Information, Figures S6, S7.

The results of the comparison between the experimental and simulated diffraction patterns are present in the Figure 5. The

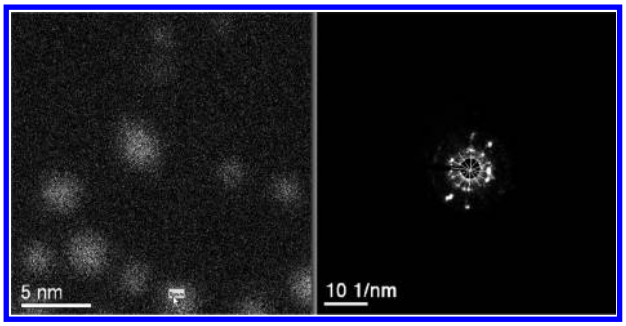


**Figure 4.** Example of STEM diffraction. In the image at left the particles do not show atomic resolution because the beam is set to produce diffraction. The marker indicates the location where the beam is directed onto the particle to obtain the diffraction pattern, at right, recorded instantaneously after putting the beam above the indicated nanocluster.

structure of the model proposed has less ligands at its ends (or poles) displaying a flattened structure. For this reason we have a good diffraction pattern near to a 5-fold symmetry. To compare the experimental results and the simulated diffraction patterns, first we measure the angles between the spots of the reflections of the experimental data, and after that we compare them with the simulated diffraction patterns. In this case Figure 5a corresponds to a single frame of video 1 of the Supporting Information. Figure 5a* shows the experimental diffraction pattern which has two distinct rings. The distance of the first one is 2.22 Å corresponding with reflections (111) in fcc notation comprised between 2.37 Å and 2.44 Å as predicted by the optimized structure model. The second ring shows a distance of 1.22 Å which corresponds to (113) in fcc notation.

To simulate the electron diffraction patterns of the proposed model, it is encapsulated in a Cartesian box using the conventional Miller indices. In this manner the cluster can be considered as a particle contained in a subspace from that ⟨UVW⟩ coordinates. By using the SimulaTEM software package,[28] we considered six different directions to rotate the simulated patterns: ⟨100⟩, ⟨010⟩, ⟨1−10⟩, ⟨110⟩, ⟨111⟩ and ⟨112⟩, each from zero to 360 degrees (see the map illustrated in the Supporting Information, Figure S5). The whole set of electron patterns simulated were integrated in a stack of images and processed to create videos 2 to 7 in the Supporting Information. It is clear that because of the reduced $D_5$ symmetry of the structure the diffraction patterns repeat several times. Unlike an infinite crystal, nanoclusters in this size show only a limited number of different diffraction patterns.[29−31]

In Table 1 are shown comparisons between simulated and measured data, and quantitative comparisons of the spot positions and angles. The ability of our method to probe individual clusters rather than data recorded as an average, over a crystal containing a large number of clusters, as in X-ray diffraction (even with bright synchrotron sources), provides the impetus for further development of the methods of data acquisition and quantitative data analysis.

We also obtained images of the clusters with atomic resolution using the STEM-HAADF with a probe corrected electron microscope. We compared calculated images based on the theoretical model with experimental ones. The HAADF-STEM simulated image has been obtained by employing the QSTEM software package[32] using parameter values matching the experimental operational conditions of the aberration-


dx.doi.org/10.1021/jp406665m | J. Phys. Chem. A 2013, 117, 10470−10476

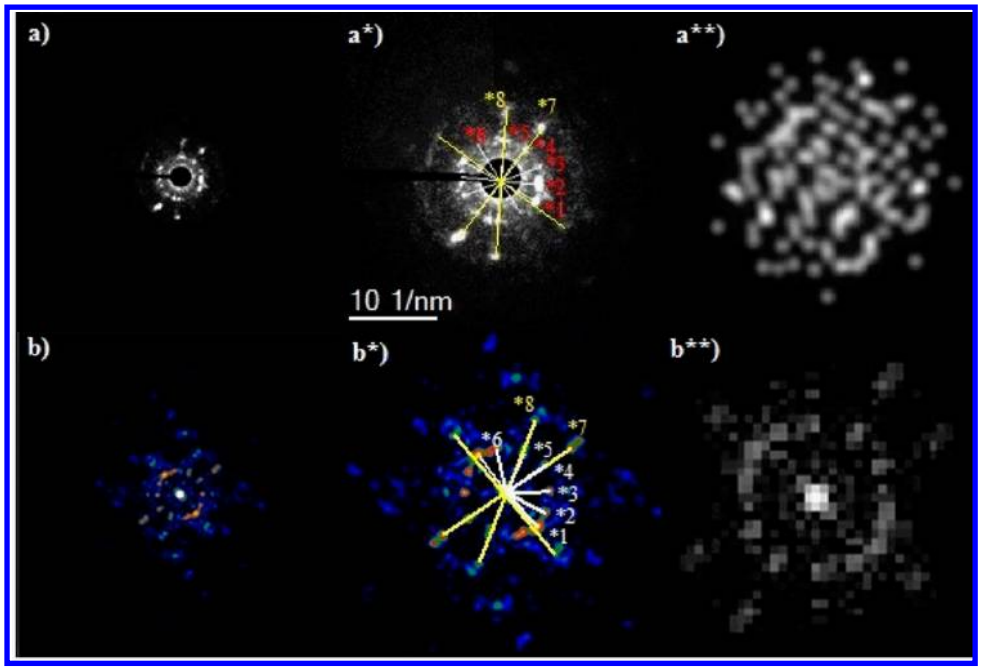


**Figure 5.** Comparison between experimental and theoretical electron diffraction patterns. In these patterns a projection with 16 reflections is observed. (a, a*) Experimental NBD pattern, cf. Figure 4b, and enlarged for marking purposes; (b, b*) as (a, a*) but for the simulated electron diffraction pattern; (a**, b**) are the simulated STEM image and 2D-FFT pattern, respectively.

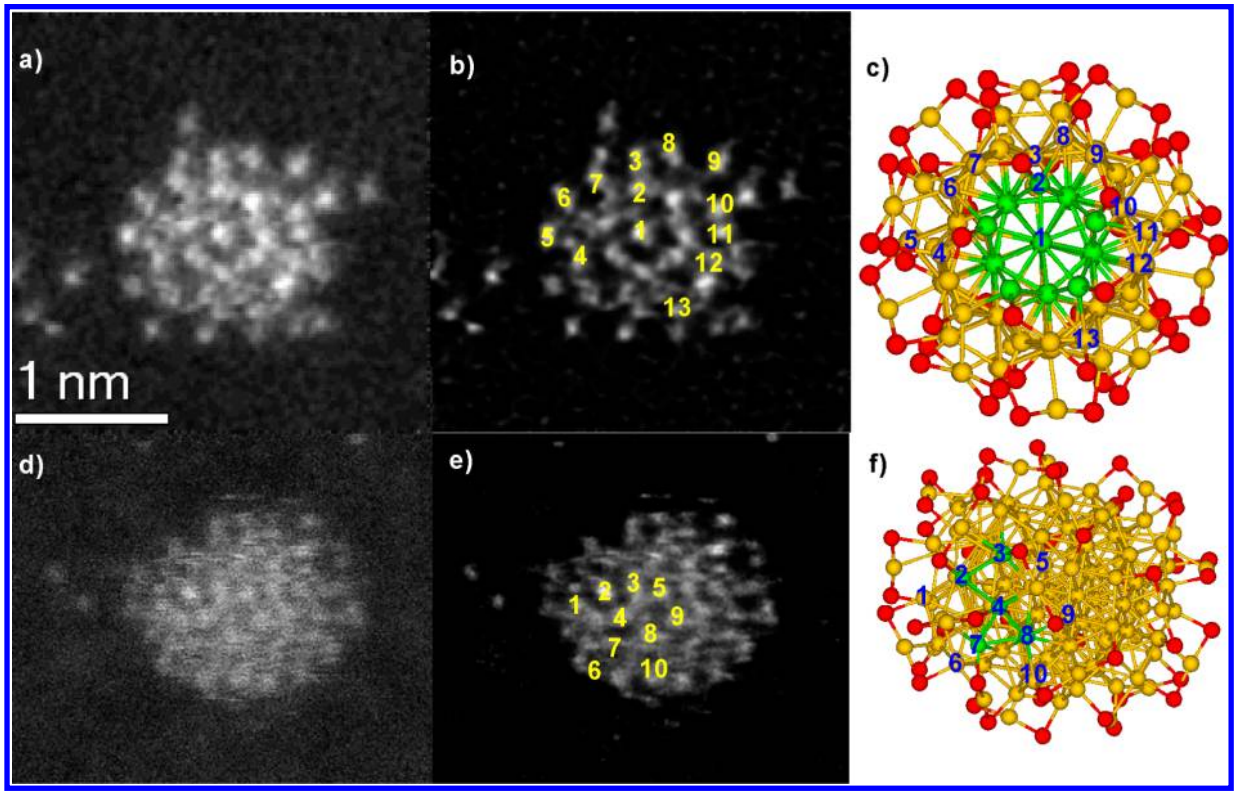


**Figure 6.** (a) HAADF image obtained at 80 kV; (b) Its deconvoluted HAADF image, calculated with the experimental microscope parameters using a personal Matlab code; (c) The structure model oriented to show the number of coincidences found between the enhanced HAADF image and the model, where gold atoms near the $C_5$ axis are colored in green, sulfur atoms are in red, and missing gold atoms are shown in yellow. In a similar manner, (d), (e), and (f) display a distinct particle oriented along a 2-fold axis.

corrected microscope. Since the DFT calculations do not include thermal effects, we have employed the appropriate Debye–Waller factors in our simulations of the data. The HAADF images with atomic resolution of the $Au_{130}$ cluster are displayed in Figures 6,7 and Supporting Information, Figure S8. They show clearly the 5-fold symmetry of the gold core, and its comparison with the relaxed model yields a stunning number of coincidences (Figure 6c). It is evident that the obtained


dx.doi.org/10.1021/jp406665m | J. Phys. Chem. A 2013, 117, 10470–10476

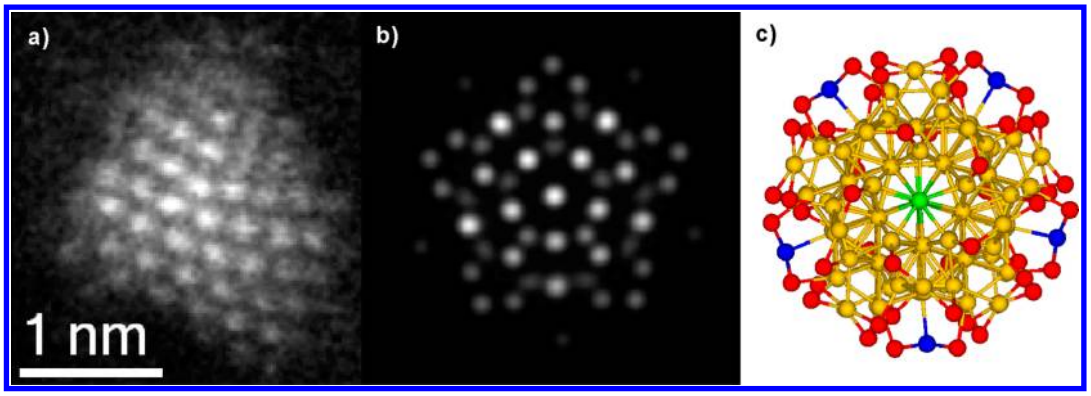


**Figure 7.** Image of a distinct particle oriented along the 5-fold axis, but with an improved view of the periphery to reveal the re-entrant Marks decahedral motif. (a) An HAADF image obtained at 80 kV; (b) Simulated image, (c) Model of the $Au_{130}(SH)_{50}$ cluster.

**Table 1. Measurements Comparing Experimental NBD-STEM and Simulated Electron Diffraction Patterns Shown in Figure 5**

| | angle (degrees) ± 2 (error) | |
|---|---|---|
| spot | experimental | theoretical |
| *1 | 23 | 21 |
| *2 | 26 | 28 |
| *3 | 32 | 36 |
| *4 | 32 | 33 |
| *5 | 36 | 39 |
| *6 | 28 | 25 |
| *7 | 33 | 34 |
| *8 | 57 | 62 |

HAADF images of the $Au_{130}$ cluster support the $Au_{75}$ Marks decahedron structure.

## 5. CONCLUSIONS

In this work, the primary focus has been to offer electron diffraction patterns and high-resolution structure imaging of the novel mixed mono/dithiolate (MT/DT) protected clusters,[15] and to give them a consistent interpretation in terms of a plausible structure and bonding model of the core and surface. The composition (130 Au; 30 DT, 20 MT) was taken to be essentially the one estimated in ref 15, whereas in the monothiolate only report of Negishi et al.,[18] the (130,50) composition was precisely determined. However, the durene-dithiolate molecular and electronic structures, as described in ref 15, were not incorporated fully into the current model, which might limit the agreement between experimental and calculated electronic structures. The possible core-ligand interactions are under further investigation.

For simplicity, we have further assumed an unorthodox bonding of the 80 thiolate sulfur-atoms: Only 50 are bonded directly to gold, whereas the remaining 30 participate in disulfide (-S-S-) linkages having no contact to gold atoms. This is the mildly oxidized form of the thiol functionality, cf. cysteine vs cystine in biochemistry, and is nowadays believed not to be stable in the presence of reduced gold Au(0), such as exists in the interior (core) of the $Au_{130}$ cluster. We have also considered other candidate structures in which all 80 thiolate S-atoms are bound in the usual bridging fashion to pairs of Au atoms or Au(I) ions. In such models there are many longer ("dimer") staples, and a correspondingly smaller core. The comparative stability and other properties of these will be discussed separately, along with the electronic structure and bonding-network properties that underlie its special stability.[33] For the present purposes, we are satisfied that the electron microscope images and diffraction patterns thus far are sensitive mainly to the core structure, and these are well reproduced by the 105-atom grand core suggested earlier by Negishi et al.[18] and as implemented in optimized form herein.

In summary, we have determined the structure of the $Au_{130}$ cluster following a previous method which is based on the combination of STEM single particle diffraction with atomically resolved images obtained through the use of STEM-HAADF, and the calculation of images and patterns based on structure models obtained and optimized via theoretical first-principles (DFT) methods. In addition, we have obtained a good agreement between calculated absorption spectrum and the experimental curve, over the entire relevant spectral range (1.5−4.0 eV), as one of the largest metallic cluster systems treated thus far by the real-time dynamics method.[34]

## ■ ASSOCIATED CONTENT

### Ⓢ Supporting Information

Experimental and calculated UV/vis spectra, MALDI-MS; theoretical model of $Au_{130}$ cluster including 80 sulfur atoms; Raman spectra and calculated XRD patterns; Atlas of simulated electron diffraction patterns and a map of simulated images; experimental NBD video; and videos of electron diffraction pattern including 6 directions. This material is available free of charge via the Internet at http://pubs.acs.org.

## ■ AUTHOR INFORMATION

### Corresponding Author

*E-mail: Robert.Whetten@utsa.edu. Phone: (210) 458-5662.

### Notes

The authors declare no competing financial interest.

## ■ ACKNOWLEDGMENTS

The authors would like to acknowledge the NSF for support with Grants DMR-1103730, "Alloys at the Nanoscale: The Case of Nanoparticles Second Phase" and PREM: NSF PREM Grant DMR 0934218; "Oxide and Metal Nanoparticles-The Interface Between Life Sciences and Physical Sciences". The MALDI TOF/TOF work is supported by the National Science Foundation under Grant CHE-1126708. The efforts at Georgia State University were supported by NSF Grant CHE-1059022. Computations were made at the Texas Advanced Computing Center (TACC).

## REFERENCES


(1) Heaven, M. W.; Dass, A.; White, P. S.; Holt, K. M.; Murray, R. W. Crystal Structure of The Gold Nanoparticle $[N(C_8H_{17})_4][Au_{25}(SCH_2CH_2Ph)_{18}]$. *J. Am. Chem. Soc.* **2008**, *130*, 3754−3755.

(2) Zhu, M.; Aikens, C. M.; Hollander, F. J.; Schatz, G. C.; Jin, R. Correlating the Crystal Structure of a Thiol-Protected $Au_{25}$ Cluster and Optical Properties. *J. Am. Chem. Soc.* **2008**, *130*, 5883−5885.

(3) Qian, H.; Eckenhoff, W. T.; Zhu, Y.; Pintauer, T.; Jin, R. Total Structure Determination of Thiolate-Protected $Au_{38}$ Nanoparticles. *J. Am. Chem. Soc.* **2010**, *132*, 8280−8281.

(4) Zeng, C.; Qian, H.; Li, T.; Li, G.; Rosi, N. L.; Yoon, B.; Barnett, R. N.; Whetten, R. L.; Landman, U.; Jin, R. Total Structure and Electronic Properties of the Gold Nanocrystal $Au_{36}(SR)_{24}$. *Angew. Chem.* **2012**, *124*, 13291−13295.

(5) Jadzinsky, P. D.; Calero, G.; Ackerson, C. J.; Bushnell, D. A.; Kornberg, R. D. Structure of a Thiol Monolayer-Protected Gold Nanoparticle at 1.1 Å Resolution. *Science* **2007**, *318*, 430−433.

(6) Mednikov, E. G.; Dahl, L. F. Crystallographically Proven Nanometer-sized Gold Thiolate Cluster $Au_{102}(SR)_{44}$: Its Unexpected Molecular Anatomy and Resulting Stereochemical and Bonding Consequences. *Small* **2008**, *4*, 534−537.

(7) Gao, Y.; Shao, N.; Zeng, X. C. Ab initio Study of Thiolate-Protected $Au_{102}$ Nanocluster. *ACS Nano* **2008**, *2*, 1497−1503.

(8) Whetten, R. L.; Price, R. C. Nano-Golden Order. *Science* **2007**, *318*, 407−408.

(9) Chaki, N. K.; Negishi, Y.; Tsunoyama, H.; Shichibu, Y.; Tsukuda, T. Ubiquitous 8 and 29 kDa Gold:alkanethiolate Cluster Compounds: Mass-Spectrometric Determination of Molecular Formulas and Structural Implications. *J. Am. Chem. Soc.* **2008**, *130*, 8608−8610.

(10) Lopez-Acevedo, O.; Akola, J.; Whetten, R. L.; Grönbeck, H.; Häkkinen, H. Structure and Bonding in the Ubiquitous Icosahedral Metallic Gold Cluster $Au_{144}(SR)_{60}$. *J. Phys. Chem. C* **2009**, *113*, 5035−5038.

(11) Qian, H.; Jin, R. Controlling Nanoparticles with Atomic Precision: The Case of $Au_{144}(SCH_2CH_2Ph)_{60}$. *Nano Lett.* **2009**, *9*, 4083−4087.

(12) Bahena, D.; Bhattarai, N.; Santiago, U.; Tlahuice, A.; Ponce, A.; Bach, S.B. H.; Yoon, B.; Whetten, R. L.; Landman, U.; Jose-Yacamán, M. STEM Electron Diffraction and High-Resolution Images Used in the Determination of the Crystal Structure of the $Au_{144}(SR)_{60}$ Cluster. *J. Phys. Chem. Lett.* **2013**, *4*, 975−981.

(13) Fields-Zinna, C. A.; Sardar, R.; Beasley, C. A.; Murray, R. W. Electrospray Ionization Mass Spectrometry of Intrinsically Cationized Nanoparticles, $[Au_{144/146}(SC_{11}H_{22}N(CH_2CH_3)_3^+)_x(S(CH_2)_5CH_3)_y]_x^+$. *J. Am. Chem. Soc.* **2009**, *131*, 16266.

(14) Qian, H.; Zhu, Y.; Jin, R. Atomically Precise Gold Nanocrystal Molecules with Surface Plasmon Resonance. *Proc. Natl. Acad. Sci. U.S.A.* **2012**, *109*, 696−700.

(15) Tang, Z.; Robinson, D. A.; Bokossa, N.; Xu, B.; Wang, S.; Wang, G. Mixed Dithiolate Durene-DT and Monothiolate Phenylethanethiolate Protected $Au_{130}$ Nanoparticles with Discrete Core and Core-Ligand Energy States. *J. Am. Chem. Soc.* **2011**, *133*, 16037−16044.

(16) Tang, Z. H.; Xu, B.; Wu, B. H.; Robinson, D. A.; Bokossa, N.; Wang, G. L. Monolayer Reactions of Protected Au Nanoclusters with Monothiol Tiopronin and 2,3-Dithiol Dimercaptopropanesulfonate. *Langmuir* **2011**, *27*, 2989−299.

(17) Tang, Z.; Ahuja, T.; Wang, S.; Wang, G. Near Infrared Luminescence of Gold Nanoclusters Affected by the Bonding of 1,4-dithiolate Durene and Monothiolate Phenylethanethiolate. *Nanoscale* **2012**, *4*, 4119−4124.

(18) Negishi, Y.; Sakamoto, C.; Tatsuya, O.; Tsukuda, T. Synthesis and the Origin of the Stability of Thiolate-Protected $Au_{130}$ and $Au_{187}$ Clusters. *J. Phys. Chem. Lett.* **2012**, *3*, 1624−1628.

(19) Perdew, P.; Burke, K.; Ernzerhof, M. Generalized Gradient Approximation Made Simple. *Phys. Rev. Lett.* **1996**, *77*, 3865−3868.

(20) Troullier, N.; Martins, J. L. Efficient pseudopotentials for Plane-Wave Calculations. *Phys. Rev. B* **1991**, *43*, 1993−2006.

(21) Soler, J. M.; Artacho, E.; Gale, J. D.; García, A.; Junquera, J.; Ordejón, P.; Sánchez-Portal, D. The SIESTA Method for Ab initio Order-N Materials Simulation. *J. Phys.: Condens. Matter* **2002**, *14*, 2745−2779.

(22) Runge, E.; Gross, E. K. U. Density-Functional Theory for Time-Dependent Systems. *Phys. Rev. Lett.* **1984**, *52*, 997−1000.

(23) Marques, M. A. L.; Castro, A.; Bertsch, G. F.; Rubio, A. octopus: a First-Principles Tool for Excited Electron-Ion Dynamics. *Comput. Phys. Commun.* **2003**, *151*, 60−78.

(24) Castro, A.; Marques, M. A. L.; Appel, H.; Oliveira, M.; Rozzi, C.; Andrade, X.; Lorenzen, F.; Gross, E. K. U.; Rubio, A. octopus: A Tool for The Application of Time-Dependent Density Functional Theory. *Phys. Status Solidi B* **2006**, *243*, 2465−2488.

(25) Perdew, J. P.; Zunger, A. Self-interaction Correction to Density-Functional Approximations for Many-Electron Systems. *Phys. Rev. B* **1981**, *23*, 5048−5079.

(26) Jupally, V. R.; Kota, R.; Dornshuld, E. V.; Mattern, D. L.; Tschumper, G. S.; Jiang, D.-E.; Dass, A. Interstaple Dithiol Cross-Linking in $Au_{25}(SR)_{18}$ Nanomolecules: A Combined Mass Spectrometric and Computational Study. *J. Am. Chem. Soc.* **2011**, *133*, 20258−20266.

(27) Tlahuice-Flores, A.; Whetten, R. L.; Jose-Yacaman, M. Ligand Effects on the Structure and the Electronic Optical Properties of Anionic $Au_{25}(SR)_{18}$ Clusters. *J. Phys. Chem. C* **2013**, DOI: 10.1021/jp407150t.

(28) Gómez-Rodríguez, A.; Beltrán-del-Río, L. M.; Herrera-Becerra, R. SimulaTEM: Multislice Simulations for General Objects. *Ultramicroscopy* **2010**, *110*, 95−104.

(29) Williams, P. Motion of Small Gold Clusters in the Electron Microscope. *Appl. Phys. Lett.* **1987**, *50*, 1760−1762.

(30) Ben-David, T.; Lereah, Y.; Deutscher, G.; Penisson, J.; Bourret, A.; Kofman, R.; Cheyssac, P. Correlated Orientations in Nanocrystal Fluctuations. *Phys. Rev. Lett.* **1997**, *78*, 2585−2587.

(31) Be'er, A.; Kofman, R.; Phillipp, F.; Lereah, Y. Spontaneous Crystallographic Instabilities of Pb Nanoparticles in a SiO Matrix. *Phys. Rev. B* **2007**, *76*, 075410−1−075410−5.

(32) Koch, C. T. Ph.D. Thesis, Arizona State University, Phoenix, Arizona, 2002.

(33) Tlahuice, A.; Black, D. M.; Bach, S. B. H.; Jose-Yacaman, M.; Whetten, R. L. Structure and Bonding of the Gold-Subhalide Cluster *I*-$Au_{144}Cl_{60}^{[z]}$. *Phys. Chem. Chem. Phys.* **2013**, DOI: 101039/C3CP53902D.

(34) Lopez-Lozano, X.; Mottet, C.; Weissker, H.-Ch. Effect of Alloying on the Optical Properties of Ag-Au Nanoparticles. *J. Phys. Chem. C* **2013**, *117*, 3062−3068.